SAND2019-14621C

Spatially-Resolved Surface Temperature Measurements of a Rocket Motor Nozzle using an Acousto-optic Modulator

Yi Chen Mazumdar*
Georgia Institute of Technology, Atlanta, GA, 30332, USA

Justin L. Wagner†, Donald J. Frederick‡, Daniel R. Guildenbecher§
Sandia National Laboratories, Albuquerque, NM, 87185, USA

Terry L. Hendricks¶
Exo-Atmospheric Technologies, LLC, Menomonee Falls, WI, 53051, USA

Solid rocket motors operate at high temperatures that can potentially damage engineering materials used for motor nozzles or thrust vanes. In this work, surface temperature measurements were collected on solid rocket motor components of varying materials exposed to the combustion of ammonium perchlorate-based solid propellants. Spatially-resolved temperatures were measured using a novel two-color pyrometer built from an acousto-optic tunable filter (AOTF) coupled to a near IR camera. Temperatures were then verified using a single-point visible spectrometers. Experiments conducted in low pressure conditions inside a high altitude chamber at Sandia National Laboratories illustrate the temporal and spatial evolution of temperature gradients across the nozzle and vanes.

I. Introduction

Solid rocket motors are commonly used to generate thrust for a variety of applications. Propellant grains based on ammonium perchlorate produce temperatures up to 1600 K at low pressures [1]. If aluminum particles are added to boost the specific impulse, atmospheric burning temperatures in the flame can be as high as 2300 to 3500 K [2–5]. Materials that interact with propellant flames must be able to operate at these extreme temperatures. However, many high temperature materials, including carbon-carbon [6], titanium [7], and rhenium [8], are either expensive or difficult to manufacture. Thus, estimating the surface temperature distributions on rocket motor nozzles and vanes is critical for monitoring temperature-related damage and for informing new designs.

There are several existing methods for measuring surface temperatures. Thermographic cameras, thermopiles, and bolometers are typically utilized to estimate two-dimensional (2D) temperature profiles at lower temperatures below $\sim$ 1000 K, because these methods typically operate in the infrared. These methods also use a single sensor to capture the optical emission intensity. Therefore, temperature estimates are sensitive to the emissivity value and must be calibrated to the exact emissivity of each material in the scene. Fluorescence, absorption, or emission spectroscopy can also be utilized to estimate surface temperatures. Fluorescence and absorption spectroscopy rely on the spectroscopic characteristics of specific materials and therefore cannot be readily applied to every surface. In some cases, however, thermographic phosphors can be painted onto materials to estimate temperatures. At extreme temperature and flow conditions on rocket motor vanes, for example, thermographic paints may be readily damaged.

Emission spectroscopy, on the other hand, can be used to directly measure material incandescence. For temperatures $\geq$800 K, the spectrum can be measured with conventional near infrared (IR) or visible spectrometers. If the material is relatively gray or black-body, then the spectrum shape can be directly related to the object temperature and no detailed information on the emissivity is required. Spectroscopy, however, is typically a single-point technique. One method for simplifying emission spectroscopy is pyrometry. In pyrometry, a minimum of two wavelength bands need to be collected and compared to determine temperature. To expand pyrometry to an imaging technique, a minimum of two images need to be collected to estimate temperature [9, 10]. This technique is especially useful for measuring multiple material with different gray body emissivities simultaneously, as long as emission peaks are avoided [11].

*Assistant Professor, Woodruff School of Mechanical Engineering, ellen.mazumdar@me.gatech.edu, Member AIAA.
†Principal Member of the Technical Staff, Engineering Sciences Center, jwagner@sandia.gov, Member AIAA.
‡Principal Member of the Technical Staff, Advanced Systems and Transformation, dfreder@sandia.gov.
§Principal Member of the Technical Staff, Engineering Sciences Center, drguild@sandia.gov, Member AIAA.
¶Chief Technology Officer, terry.hendricks@exo-at.com.

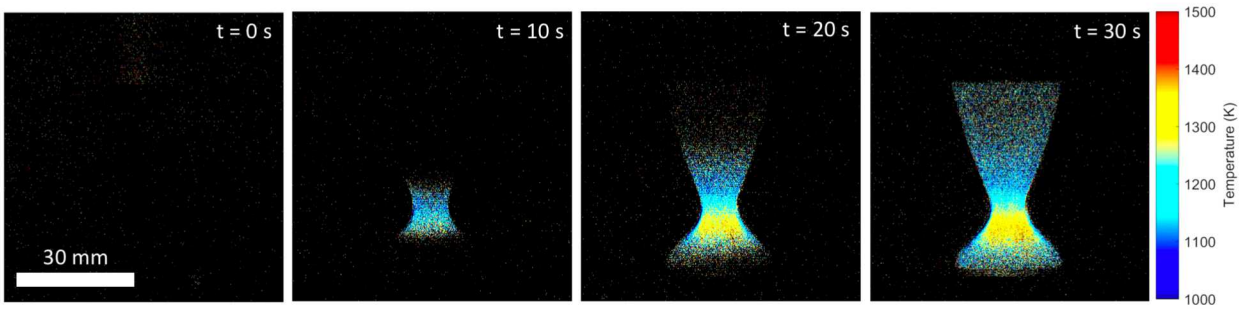

Fig. 1 Temperature change as a function of time of a nozzle during a solid rocket propellant burn in a high altitude chamber. Two-dimensional temperature profiles are estimated using AOTF imaging pyrometry.

Pyrometry imaging systems typically use two or more cameras and thus alignment of the two images is critical [3, 12]. Because the two images are taken at different wavelengths, it is also challenging to obtain the same focus on both cameras. In this work, we propose a novel, alternative technique that uses an acousto-optic tunable filter (AOTF) and a single near IR camera for pyrometry to estimate surface temperatures of solid rocket motor components. This technique requires only a single camera with snapshots taken at 700 nm and 850 nm, which greatly simplifies alignment and space requirements. This small and robust apparatus is then placed inside a sealed container for use in a large high-altitude vacuum chamber for rocket motor testing. The temperature change of a rocket motor nozzle as a function of time is illustrated in Fig. 1. Results are then calibrated against a black body source and compared with emission spectroscopy measurements.

II. Experimental Setup

In order to test rocket motor combustion at application relevant conditions, experiments were conducted in large vacuum chambers. Preliminary experiments were implemented in a 1.5 m diameter LACO vacuum chamber with large external view ports. For the final experiments, the High Altitude Chamber (HAC) at Sandia National Laboratories was used. The HAC is a vacuum sphere with an inner diameter of 8.2 m and can simulate altitudes of up to ~70,000 m (~230,000 feet), pumping down within 20 minutes. An image of the HAC interior is shown in Fig. 2 on the right.

The AOTF imaging pyrometer schematic is shown in the left-most portion of Fig. 2. The pyrometer consists of a variable focus lens (f/8 maximum aperture), a Brimrose AOTF (VA310-.55-1.0) and a near IR camera (Manta G-145 NIR, 12-bit, 1388 × 1038 pixels, 6.45 μm pixel size, 33 dB gain max). The Brimrose AOTF is composed of a series of lenses and polarizers along with an acousto-optic modulator (AOM). By varying the AOM driving frequency, different wavelengths are selectively transmitted to the near IR camera with a bandwidth ranging from 1.5 to 7 nm depending on the wavelength. Reliable synchronization of the AOTF and camera was achieved at a rate of 9 Hz using a custom LabVIEW program. For final testing, alternating image patterns were collected at 700 and 850 nm. Additional black

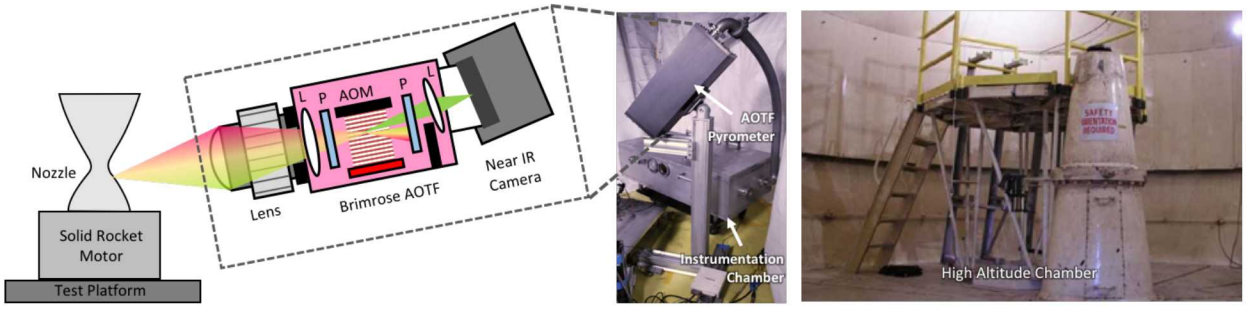

Fig. 2 The AOTF imaging pyrometer (left) is placed inside a vacuum-proof box connected to an instrumentation chamber (middle). The entire setup is placed inside the high altitude vacuum chamber (right). (L–lens; P–polarizer, AOM–acousto-optic modulator)

synchronization frames were also captured by reducing the modulation amplitude on the AOM.

To protect the drive electronics from vacuum conditions and the soot produced by the propellant, the imaging system was placed inside a custom sealed box tilted downward as illustrated in the middle of Fig. 2. The umbilical cord containing the cables was then routed to an additional instrumentation box, which contained power and drive electronics. The instrumentation box also protected a visible spectrometer (Ocean Optics USB2000+) pointed toward the rocket motor nozzle from the main view point. A separate near IR scanning spectrometer (Spectralline model ES200, 1.2 to 4.6 μm range) and several other visible wavelength monitoring cameras were placed around the test platform at different locations. During experiments, the HAC was pumped down to different altitudes and the monitoring instrumentation was turned on before the main propellant grain was ignited utilizing smaller igniter grains. When the igniter grain (metalized) was started, a small puff of propellant smoke can be seen on the AOTF imaging pyrometer, aiding in the determination of relative timing. Various main propellant grain types (not metalized) with total burn durations between 10 to 45 seconds were utilized. The combustion gases from the main grain were generally not visible on the AOTF pyrometer due to the low gas densities at the outlet.

III. Temperature Estimation and Calibration

Pyrometry requires a minimum of two wavelengths to be collected and compared to estimate temperature. Assuming gray or black body thermal emission from the nozzle and vanes, Planck's equation can be used. If $hc/\lambda \gg kT$, then Wien's approximation,

$$I \approx \frac{2hc^2\epsilon}{\lambda^5} e^{-\frac{hc}{\lambda kT}}, \tag{1}$$

can be used to simplify temperature estimates. Here h is Planck's constant, c is the speed of light, ϵ is the emissivity, λ is the wavelength, k is the Boltzmann constant, and T is the temperature. The ratio of intensities at each pixel from two images $R = (I_2\eta_1\zeta_1)/(I_1\eta_2\zeta_2)$ can then be estimated, where ζ is the quantum efficiency and η is the exposure length. The temperature at each pixel can then be calculated as,

$$T = \left[\frac{k}{hc}\frac{\lambda_1\lambda_2}{\lambda_2-\lambda_1}\left(ln(R) - 5ln\left(\frac{\lambda_1}{\lambda_2}\right)\right)\right]^{-1}. \tag{2}$$

The selection of the two wavelengths used for pyrometry is an important consideration. The wavelengths must be free of emission peaks and sufficiently far apart to produce high sensitivity temperature estimates. However, they must also be chosen to maximize the collection efficiency within the expected temperature range. The wavelengths must also be sufficiently close together such that the emissivities [6–8] are similar and thus cancel in Eq.(2). For the experiments described in this paper, wavelengths of 700 and 850 nm were selected balancing these factors.

Although quantum efficiencies can be calculated, it is also possible to calibrate the entire imaging system using a black body source. Here, a 25 mm diameter black body source (Infrared Systems Development Corp. IR-564/301) was

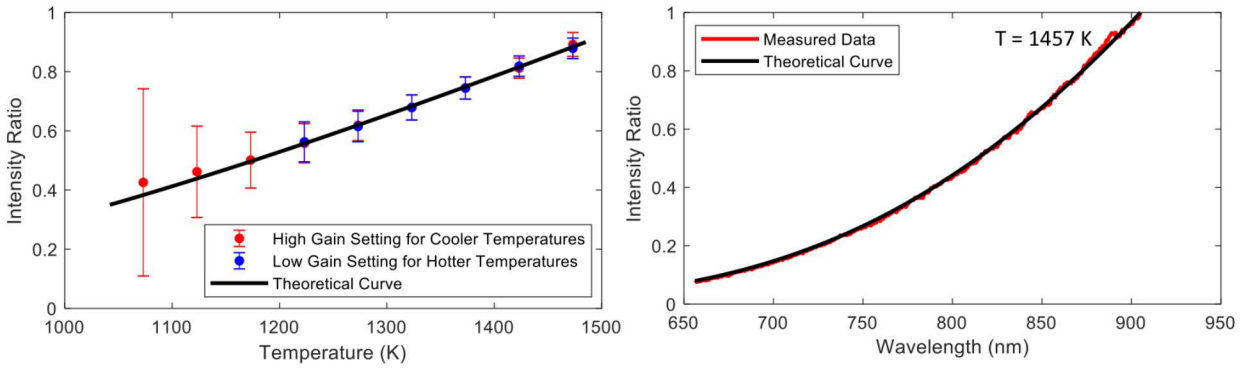

Fig. 3 Calibrations of the AOTF pyrometer (left) and visible spectrometer at T = 1457 K (right) against a black body source are shown. These are compared with the best-fit theoretical curves from Eq.(2). For the AOTF calibrations, error bars indicate intensity ratio variation across the 25 mm source. The high and low gains correspond to a 16 and 3 dB gain settings on the camera, respectively.

set between ~1000 and ~1500 K to calibrate both the AOTF pyrometer and the visible spectrometer, as shown in Fig. 3. These calibrations were then matched to best-fit theoretical curve from Eq.(2). By increasing the camera gain, it is possible to measure lower temperatures but at the cost of greater estimation uncertainty. Therefore, lower gain values are used where possible.

IV. Experimental Results

A. AOTF Imaging Pyrometry

The AOTF imaging pyrometer was utilized to measure several different rocket motor configurations. Figure 4 shows two sequential images taken at two wavelengths while looking down on the rocket motor nozzle and four control vanes. It is important to note that images at different wavelengths can be shifted vertically on the camera due to the AOTF topology and external vibrations. Thus, non-physical temperature gradients can be seen at object edges, including the bottom edges of the vanes. It is also important to note that metal components can also reflect hotter emissions, which can be seen on the metal ring surrounding the nozzle throat, showing a higher temperature only in regions facing the nozzle. Overall, temperature contours on the nozzle and across the vanes can be clearly seen smoothly transitioning from hot regions on the vanes near the nozzle centerline to colder regions on the vanes near the vane control motors.

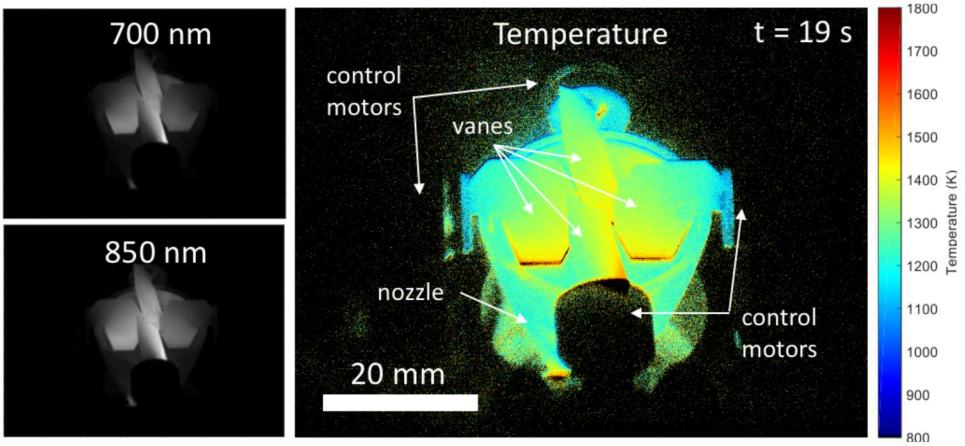

Fig. 4 AOTF imaging pyrometry of a rocket motor nozzle and four control vanes. Two images taken at 700 and 850 nm (left) are combined to generate a single calibrated temperature image (right).

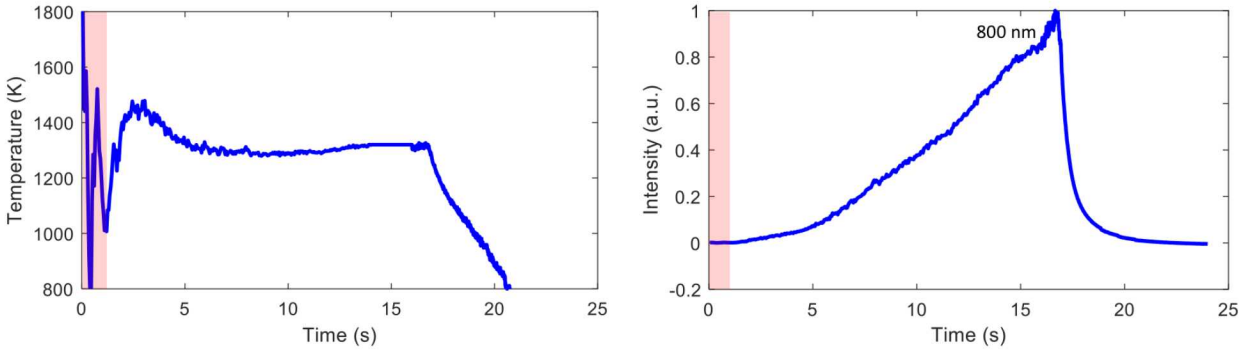

Fig. 5 Fitted temperature (left) and intensity at 800 nm (right) as a function of time measured with a visible spectrometer pointed at the nozzle throat. The red boxes indicate regions of low estimation confidence due to low light intensities.

B. Visible Spectroscopy

The nozzle temperature can also be estimated using the visible spectrometer. The time-resolved temperature estimate and intensity increase over time are shown in Fig. 5. In this figure, the red regions indicates areas where the temperature estimation confidence is low due to low intensities. As time increases, the temperature at the outside of the nozzle throat stays between 1280 and 1460 K, which matches well with estimates illustrated earlier in Fig. 1 and 4. The measured intensity, however, grows as a function of time as the temperature distributes across the nozzle. When the propellant grain burns out, the temperature and intensity rapidly decrease.

V. Conclusion

In this work, we describe a new method for collecting imaging pyrometry measurements in a high altitude vacuum facility using an acousto-optic modulator and a single near-IR cyhamera. This system collects images at different wavelengths and ratios the measurements to produce two-dimensional measurements of surface temperature. Switching between different wavelengths makes this measurement method inherently slow compared to other single-shot imaging pyrometer techniques [3]. However, the switching speed of the AOM is sufficiently fast to capture the temperature dynamics of a small rocket motor nozzle. Overall, this technique has shown great promise in this facility due to its minimal re-alignment requirements and its ability to capture surface temperatures of multiple gray-body materials simultaneously. In the future, we aim to study this rocket motor system further by conducting time-resolved analysis, studying the influence of different sources of uncertainty, and comparing AOTF pyrometer and IR spectrometer results.

Acknowledgments

The authors would like to thank Russel Spillers, Seth Spitzer and Paul Farias for their help setting up experiments. Sandia National Laboratories is a multimission laboratory managed and operated by National Technology and Engineering Solutions of Sandia, LLC., a wholly owned subsidiary of Honeywell International, Inc., for the U.S. Department of Energy's National Nuclear Security Administration under contract DE-NA0003525.

References

[1] Powling, J., and Smith, W., "The surface temperature of burning ammonium perchlorate," *Comb. Flame*, Vol. 7, 1963, pp. 269–275.

[2] Kearney, S. P., and Guildenbecher, D. R., "Temperature Measurements in Metallized Propellant Combustion using Hybrid fs/ps Coherent Anti-Stokes Raman Scattering," *Appl. Opt.*, Vol. 55, No. 18, 2016, pp. 4958–4966.

[3] Chen, Y., Guildenbecher, D. R., Hoffmeister, K. N. G., Cooper, M. A., Stauffacher, H. L., Oliver, M. S., and Washburn, E. B., "Study of Aluminum Particle Combustion in Solid Propellant Plumes using Digital In-line Holography and Imaging Pyrometry," *Combust. Flame*, Vol. 182C, 2017, pp. 225–237.

[4] Chen, Y., Guildenbecher, D. R., Hoffmeister, K. N. G., and Sojka, P. E., "Digital Imaging Holography and Pyrometry of Aluminum Drop Combustion in Solid Propellant Plumes," *Proceedings of the Imaging and Applied Optics Conference: Laser Applications to Chemical, Security and Environmental Analysis*, 2016. LT4F.2.

[5] Chen, Y., Heyborne, J. D., and Guildenbecher, D. R., "Time-resolved Digital In-line Holography and Pyrometry for Aluminized Solid Rocket Propellants," *Proceedings of the Imaging and Applied Optics Conference: Laser Applications to Chemical, Security and Environmental Analysis*, 2018. LTu3C.5.

[6] Balat-Pichelin, M., Robert, J., and Sans, J., "Emissivity measurements on carbonŰcarbon compositesat high temperature under high vacuum," *Appl. Surf. Sci.*, Vol. 253, 2006, pp. 778–783.

[7] Bradshaw, F. J., "The Optical Emissivity of Titanium and Zirconium," *Proc. Phys. Soc. B*, Vol. 53, 1950, pp. 573–577.

[8] Marple, D. T. F., "Spectral Emissivity of Rhenium," *J. Opt. Soc. Am.*, Vol. 46, No. 7, 1958, pp. 490–494.

[9] Brazyn, T., Krier, H., and Glumac, N., "Combustion of nanoaluminum at elevated pressure and temperature behind reflected shock waves," *Combust. Flame*, Vol. 145, No. 4, 2006, pp. 703–713.

[10] Panagiotou, T., Levendis, Y., and Delichatsios, M., "Measurements of Particle Flame Temperatures Using Three-Color Optical Pyrometry," *Combust. Flame*, Vol. 104, No. 3, 1996, pp. 272–287.

[11] McNesby, K. L., Homan, B. E., Benjamin, R. A., Boyle, V. M., Densmore, J. M., and Biss, M. M., "Quantitative imaging of explosives with high-speed cameras," *Rev. Sci. Instrum.*, Vol. 87, 2016, p. 051301.

[12] Barkley, S. J., Zhu, K., Ballestero, M., Michael, J. B., and Sippel, T. R., "Microwave Seeded Plasma Enhancement of Composite Propellant Flame Temperature," *52nd AIAA/SAE/ASEE Joint Propulsion Conference*, 2016. AIAA 2016-5114.